Effect of metal dispersion and support structure of Ni/silicalite-1 catalysts on non-thermal plasma (NTP) activated CO2 hydrogenation

Chen, Huanhao; Goodarzi, Farnoosh; Mu, Yibing; Chansai, Sarayute; Mielby, Jerrik Jørgen; Mao, Boyang; Sooknoi, Tawan; Hardacre, Christopher; Kegnæs, Søren; Fan, Xiaolei

Published in:
Applied Catalysis B: Environmental

Link to article, DOI:
10.1016/j.apcatb.2020.119013

Publication date:
2020

Document Version
Peer reviewed version

Journal Pre-proof

Effect of Metal Dispersion and Support Structure of Ni/Silicalite-1 Catalysts on Non-Thermal Plasma (NTP) Activated CO_2 Hydrogenation

Huanhao Chen, Farnoosh Goodarzi, Yibing Mu, Sarayute Chansai, Jerrik Jørgen Mielby, Boyang Mao, Tawan Sooknoi, Christopher Hardacre, Søren Kegnæs, Xiaolei Fan

PII: S0926-3373(20)30428-8

DOI: https://doi.org/10.1016/j.apcatb.2020.119013

Reference: APCATB 119013

To appear in: *Applied Catalysis B: Environmental*

Received Date: 31 January 2020

Revised Date: 9 April 2020

Accepted Date: 14 April 2020

Please cite this article as: Chen H, Goodarzi F, Mu Y, Chansai S, Mielby JJ, Mao B, Sooknoi T, Hardacre C, Kegnæs S, Fan X, Effect of Metal Dispersion and Support Structure of Ni/Silicalite-1 Catalysts on Non-Thermal Plasma (NTP) Activated CO_2 Hydrogenation, *Applied Catalysis B: Environmental* (2020), doi: https://doi.org/10.1016/j.apcatb.2020.119013

Effect of Metal Dispersion and Support Structure of Ni/Silicalite-1 Catalysts on Non-Thermal Plasma (NTP) Activated CO_2 Hydrogenation

Huanhao Chen [a], Farnoosh Goodarzi [b], Yibing Mu [a], Sarayute Chansai [a], Jerrik Jørgen Mielby [b], Boyang Mao [c], Tawan Sooknoi [c,d], Christopher Hardacre [a,*], Søren Kegnæs [b,*], Xiaolei Fan [a,*]

[a] *Department of Chemical Engineering and Analytical Science, School of Engineering, The University of Manchester, M13 9PL, United Kingdom*
[b] *DTU Chemistry, Technical University of Denmark, Kemitorvet 207, 2800 Kgs, Lyngby, Denmark*
[c] *Department of Engineering, University of Cambridge, JJ Thomson Avenue, Cambridge CB3 0FA, United Kingdom*
[d] *Catalytic Chemistry Research Unit, Faculty of Science, King Mongkut's Institute of Technology Ladkrabang, Bangkok 10520, Thailand*
[e] *Department of Chemistry, Faculty of Science, King Mongkut's Institute of Technology Ladkrabang, Bangkok 10520, Thailand*

*corresponding author: c.hardacre@manchester.ac.uk (CH); skk@kemi.dtu.dk (SK); xiaolei.fan@manchester.ac.uk (XF)

Graphical Abstract

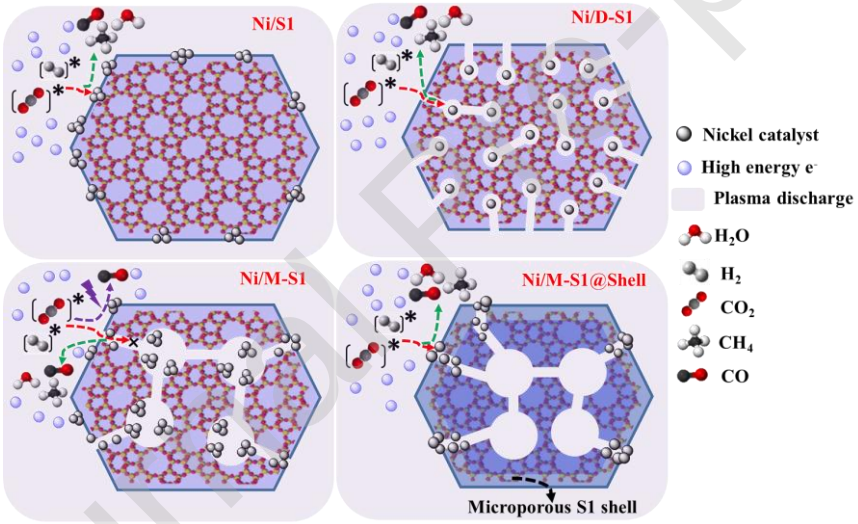

Highlights:

- Ni dispersion and location depend on the porous structure of silicalite-1
- Accessibility of active Ni sites to NTP-induced reactive species is important
- Hierarchical porous network is beneficial to NTP-activated CO_2 hydrogenation

Abstract: Non-thermal plasma (NTP) activated heterogeneous catalysis is a promising alternative to thermal catalysis for enabling many challenging reactions (*e.g.* catalytic CO_2 hydrogenation) under mild conditions. However, the mechanistic insight into the interaction between highly

energetic electrons and vibrationally-exited reactive species with metal catalyst is still lacking. Here, catalytically active Ni nanoparticles supported on silicalite-1 zeolites with different configurations regarding the location of Ni active sites and support pore structures were comparably investigated using catalytic CO_2 hydrogenation under the thermal and NTP conditions. Experimental results revealed that the performance of the NTP-catalysis depends on the configuration of the catalysts significantly. Specifically, catalysts with Ni active sites sit on the outer surface of zeolite crystals (*i.e.* microporous Ni/S1 and Ni/M-S1@Shell with steam-assisted recrystallised micro-meso-porous structure) showed relatively good catalytic performance at a low applied voltage of 6.0 kV. Conversely, the encapsulated catalyst with hierarchical meso-micro-porous structure (*i.e.* Ni/D-S1) which has relatively small (*i.e.* average Ni particle sizes of 2.8±0.7 nm) and dispersed Ni nanoparticles (*i.e.* Ni dispersion of *ca.* 2.5%) demonstrated comparatively the best catalytic performance (*i.e.* CO_2 conversion of *ca.* 75%) at 7.5 kV. Additionally, under the NTP conditions studied, Ni on carbon-templated mesoporous silicalite-1 (Ni/M-S1) showed the worst selectivity to CH_4, which was attributed to the poor accessibility of Ni active sites encapsulated in the enclosed mesopores. This study demonstrated the crucial role of catalyst design in NTP activated catalysis.

Keywords: Non-thermal plasma (NTP); Heterogeneous catalysis; Metal dispersion; Silicalite-1 zeolite; CO_2 hydrogenation

1. Introduction

Non-thermal plasma (NTP) is a promising technology which can promote challenging heterogeneous catalytic reactions such as catalytic carbon dioxide (CO_2) hydrogenation [1-3]. NTP activated heterogeneous catalysis has been demonstrated as an effective alternative to conventional thermal catalyis due to the unique interplay between the plasma and heterogeneous catalyst. Specifically, NTP helps to overcome the kinetic limitation which exist in conventional thermal catalysis without external heat sources [4, 5]. For example, Stere *et al.* applied NTP activation to enable water-gas shift (WGS) reaction for the hydrogen production over the $Au/CeZrO_4$ catalyst at low bulk temperature of ~115 °C [6]. Relevant findings suggest the possible activation of H_2O by plasma, and hence reducing the overall activation barrier and enabling the reaction at low temperatures. Vakili *et al.* [7] measured the improved conversions of methane (CH_4) and CO_2 (*i.e.* by *ca.* 18% and 10%, respectively, compared to a NTP-alone system) for catalytic dry reforming of methane (DRM) over a metal-organic framework (MOFs)-based catalyst (Pt@UiO-67) under NTP conditions. Recently, Wang *et al.* [8] also demonstrated that, under the NTP condition, $Cu/\gamma\text{-}Al_2O_3$ catalysts are able to promote CO_2 hydrogenation to methanol, being advantageous than the

traditional high-reaction temperature/-pressure catalytic processes. However, NTP-catalyst systems are highly complex due to the interaction between highly energetic electrons and vibrationally excited species and catalyst.

Accordingly, many efforts have been made to study the NTP-catalyst systems, especially using *in situ* characterisation, aiming to gain the mechanistic understanding of the complexity between plasma and heterogeneous catalyst, which can enable the rational design of new catalysts for NTP and NTP catalytic reactors. A number of advanced techniques have been developed to identify the short-lived species produced by NTP, which may play a key role in NTP catalysis. For example, isotopically-labelled molecular oxygen was employed to demonstrate that the plasma promoted the interaction of oxygen species with the surface of the Ag catalyst in catalytic oxidation of volatile organic compound (VOC) under NTP conditions [9]. Electron paramagnetic resonance (EPR) spectroscopy was also applied to examine the generation of radical species and the structural changes of the catalyst induced by NTP [10].

The property of catalysis/catalyst under NTP conditions was investigated as well. A recent study by Gibson *et al.*[11] investigated the NTP activated methane (CH_4) oxidation over the Pd/Al_2O_3 catalyst using extended X-ray absorption fine structure (EXAFS) spectroscopy. *In situ* EXAFS characterisation revealed that structural changes of the catalyst were insignificant under NTP conditions. Additionally, the authors also proposed that the NTP-induced formation of CH_3 (g) species enabled the oxidation of CH_4 *via* an alternative reaction pathway with the low activation barrier. Additionally, *in situ* diffuse reflectance infrared Fourier transform spectroscopy (DRIFTS) characterisation is also highly beneficial to the understanding of surface dynamics of the catalyst under NTP conditions, which has been recently demonstrated for various NTP-catalyst systems such as selective catalytic reduction (SCR) of NO_x [12], WGS [6, 13], DRM [14] and catalytic CO_2 hydrogenation [1-3]. Facilitated by *in situ* DRIFTS, key surface intermediates adsorbed on catalyst surface were revealed under NTP conditions, and thus contributing to the discovery and understanding of possible reaction pathways. For example, our recent study suggested the possible co-existence of the Langmuir-Hinshelwood and Eley-Rideal mechanisms in the NTP-catalyst system for catalytic CO_2 methanation (over Ni supported on BETA zeolite catalysts) due to the presence of dissociated H species in the gas phase [1] .

In addition to *in situ* characterisation, other experimental methods were also proposed to study the perturbation effect of NTP on catalysis. Kinetic study of CH_4 activation over Ni catalysts under NTP conditions was carried out by Kim *et al.* [15], and the findings suggested that the vibrationally excited CH_4 species created by plasma can favourably interact with Ni catalysts, and thus help to reduce the energy barrier required for activating CH_4. Parastaev *et al.* [4] recently developed a temperature-programmed plasma surface reaction (TPPSR) method which can decouple the gas-

phase reactions from the plasma-induced catalyst surface reactions (exemplified by catalytic CO_2 hydrogenation over $Co/CeZrO_4$ catalyst) under NTP conditions. By coupling TPPSR with isotopically labelled CO_2, the electron-excited gas-phase CO_2 dissociation was identified as the major contributor to accelerate the surface reaction *via* a low-temperature (bulk) reaction pathway.

Despite the number of studies performed, to date, the fundamental information regarding the behaviour of the reactive species generated by NTP in the gas-phase, and how the species interact with the heterogeneous catalyst is still lacking. The lifetime of plasma-induced reactive species is a key factor of NTP-catalyst systems, which ranges from nanoseconds (for electronically excited atoms/molecules) to microseconds (for radicals) [16]. Hence, the short-lived plasma-produced reactive species may only access the boundary layer of the catalyst surface, potentially participating in the reaction *via* the Eley-Rideal mechanism. Outside of the boundary layer, plasma-induced species may react or deactivate quickly in the gas-phase. Christensen *et al.* [17] detected the existence of a liquid-surface boundary layer (by *in situ* Fourier-transform infrared spectroscopy (FTIR)) on the surface of Macor catalyst during catalytic DRM under NTP, being potentially important for the formation of species such as chain oxides Ketene and C_5O_2. Therefore, the accessibility of the metal active sites in a heterogeneous catalyst is important to the performance of NTP-catalyst systems. Porous materials are commonly applied as the catalyst supports. Under an NTP, the effect of the porous network on the diffusion of plasma-induced species needs to be understood for the bespoke design of the NTP catalysts. Microporous supports are generally believed to hinder the plasma penetration and diffusion of short-lived reactive species. Therefore, the presence of mesoporous structures in microporous catalyst supports, especially hierarchical mesopores, may be beneficial to the catalysis under NTP conditions, in which the diffusion of the plasma-generated reactive species can be improved.

Herein, siliceous silicalite-1 zeolites with different pore structures (microporous, desilicated hierarchical meso-micro-porous, carbon-templated mesoporous and steam-assisted recrystallised micro-meso-porous networks) were prepared and used to support Ni nanoparticles. The effect of the porous structure of the supports on the characteristics of the supported Ni species (such as the location and dispersion of Ni species in the catalysts) was characterised in detail. The catalysts were then used in the comparative investigation of catalytic CO_2 hydrogenation under both thermal and NTP conditions, aiming to gain insight into the effect of the characteristics of the developed supported Ni catalysts on the NTP activated catalysis.

2. Experimental

2.1. Preparation of catalysts

Preparation of microporous silicalite-1 (*S1*)*:* Following the synthesis described by Goodarzi *et al* [18]. 4.46 ml of tetraethyl orthosilicate (TEOS, Sigma-Aldrich, ≥99.0%) was added dropwise to 7.26 ml solution of tetrapropylammonium hydroxide (TPAOH, Sigma-Aldrich, 1.0 M in H_2O) under stirring in a Teflon beaker. The mixture was stirred for 1 h and then heated in a Teflon-lined stainless-steel autoclave at 180 °C for 24 h. The solid product was separated by filtration from the liquid, washed several times with distilled water, dried at 80 °C overnight and then calcined for 20 hours at 550 °C.

Preparation of desilicated hierachical silicalite-1 (*D-S1*)*:* Following the previously optimised procedure [19], 0.7 g of cetyl trimethylammonium bromide (CTAB, as surfactant) was added to 50 ml of dilute aqueous ammonia solution (15%) in a Teflon beaker and stirred until complete dissolution of the surfactant. Then, 1.0 g of as-synthesised silicalite-1 was added to the solution and stirred for 3 h at room temperature. The mixture was transferred into an autoclave and heated at 90 °C for 24 h. The solid product was separated from the liquid by centrifugation and washed with distilled water. After drying the product overnight at 80 °C, the final powder was obtained by calcination at 550 °C for 10 h.

Preparation of mesoporous silicalite-1 (*M-S1*)*:* Carbon black particles (BP-2000), with average particle diameter of 12 nm, were used as a hard template for synthesis of mesoporous silicalite-1 based on synthesis methods reported by Jacobsen *et al* [20]. and Mielby *et al* [21]. The carbon black was dried at 80 °C for 24 h. Then 2.0 g of carbon black was impregnated with 7.26 ml TPAOH in a Teflon beaker and dried over night at room temperature. The dried mixture was impregnated with 4.46 ml TEOS and dried overnight again at room temperature. Then the beaker was placed in a Teflon-lined stainless-steel autoclave, and 15 ml of distilled water was added into the autoclave, around the beaker, to produce saturated steam. The autoclave was heated at 180 °C for 72 h. After the autoclave was quenched, synthesised powder was collected, washed with distilled water, dried at 80 °C for 24 h and finally calcined at 550 °C for 20 h.

Preparation of steam-assisted recrystallised mesoporous-microporous silicalite-1 (*M-S1@Shell*)*:* Following the procedure reported by Rasmussen *et al.* [22], the as-prepared mesoporous silicalite-1 was dried in vacuum oven overnight at 50 °C to dehydrate the powder. 2.0 g of mesoporous silicalite-1 was transferred into a Teflon beaker, impregnated with 7.26 ml TPAOH, and dried overnight at room ambient. The mixture was impregnated with 4.46 ml TEOS and dried again overnight. Finally, the Teflon beaker containing the mixture was transferred into a Teflon-lined stainless-steel autoclave and added 15 ml distilled water between the beaker walls. The autoclave was heated at 180 °C for 72 h followed by quenching and washing the produced powder with distilled water. The obtained solid product was dried overnight and calcined at 550 °C for 20 h.

Preparation of catalysts: Nickel nitrate ($Ni(NO_3)_2 \cdot 6H_2O$) was used as the nickel precursor in the impregnation method for supporting Ni catalysts on the supports. The dried zeolites (under vacuum overnight) were added into nickel nitrate solution under vigorously stirring at room temperature. The impregnated powder was dried in an oven at 80 °C for 12 h. Then the powder was reduced under H_2 flow (10% H_2 in nitrogen) for 2 h at 50 °C (heating ramp was 5 °C min^{-1}).

2.2. Characterisations of materials

Powder X-ray diffraction (XRD) analysis was performed on a focusing quartz monochromator and a HUBER G670 Guinier camara in transimission mode using CuKα radiation. All XRD paterns of materails presented in this work are as-recorded without background correction. Nitrogen (N_2) physisorption was carried out at liquid nitrogen temperature on a Micromeritics 3Flex Surface Characterisation Analyser. Approximately 50–100 mg was weighted and outgassed under vacuum at 400 °C overnight prior to the measurement. The specific surface area (S_{BET}) was calculated using the Brunaur-Emmett-Teller (BET) method, the total pore volumes (V_{total}) was calculated based on the amount of adsorbed N_2 at the relative pressure of $P/P^0 = 0.95$, and the micropore volume (V_{micro}) was calculated using the *t*-plot method. Scanning electron microscopy (SEM) was performed on a FEI Quanta 200 ESEM FEG operated at 10–20 kV. All samples were dispersed on carbon tape and coated with Au prior to analysis. Transmission electron microscopy (TEM) was performed on a FEI Tecnai T20 G2 microscope operated at 200 kV to investigate crystal sizes and morphology of the samples. H_2 pulse chemisorption for determining the Ni dispersion was performed on a Micromeritics AutoChem II 2920 instrument. The samples were pre-reduced at 450 °C for 1 h in a 10% H_2/Ar flow (30 mL min^{-1}) and then cooled down to 50 °C. The H_2 pulse chemisorption was then carried out by pulsing a mixture of 10% H_2/Ar (30 mL min^{-1}).

2.3. Catalytic CO_2 hydrogenation under thermal and NTP conditions

Catalytic CO_2 hydrogenation over different catalysts under thermal conditions (at atmospheric pressure) was performed in a continuous-flow cylindrical quartz reactor (6 mm O.D. × 4 mm I.D.) equipped with a K-type thermocouple for measuring the actual bed temperature. In a typical experiment, 100 mg of pelletised catalyst (particle size in a range of 250–425 μm) was packed in the reactor and reduced at 500 °C for 2 h in a 10% H_2/Ar gas flow (flow rate = 50 mL (STP) min^{-1}). After reduction, the reactor was cooled down to 250 °C in a pure Ar flow, and then a H_2/CO_2 mixture (molar composition = 4) was introduced into the reactor *via* two mass flow controllers (Bronkhorst®, F-201CV-500-RAD-11-V) at the gas hourly space velocity (GHSV) of 30,000 mL (STP) g_{cat}^{-1} h^{-1} to start the reaction. For each test, the catalysts were evaluated at different temperature varied from 250 to 500 °C. *In situ* diffuse reflectance infrared Fourier-transform

spectroscopy-mass spectrometry (DRIFTS-MS) characterisation of the catalysis over the developed catalysts was performed with the detailed procedure described elsewhere [1, 23]. Specifically, for each experiment, the catalyst was loaded into a ceramic crucible in the IR cell and reduced (at 400 °C in a 10% H_2/Ar flow for 1 h then cooled to 40 °C). Subsequently, the gas mixture (10% CO_2 + 40% H_2 with Ar balance, at 50 mL min^{-1}) was introduced, and DRIFTS spectra were recorded by ramping the temperature from 40 to 400 °C at 5 °C min^{-1}. The gases at the outlet of the DRIFTS cell were analysed by MS with the response time of <1 s. NTP activated CO_2 hydrogenation was performed in a continuous-flow dielectric barrier discharge (DBD) plasma reactor at atmospheric pressure without an external heat source. The details of DBD plasma reactor have been described elsewhere [1]. In a typical experiment under the NTP condition, 100 mg of pelletised catalyst (250–425 μm) was packed in the DBD plasma reactor and reduced at 500 °C for 2 h in a 10% H_2/Ar gas flow (flow rate = 50 mL (STP) min^{-1}, previous research has confirmed that the reducing condition was able to fully reduce the catalyst [18]). After reduction, a H_2/CO_2 mixture (molar composition = 4) was introduced into the DBD plasma reactor at GHSV = 30,000 mL (STP) g_{cat}^{-1} h^{-1}. Varied applied peak voltages from 6.0 to 7.5 kV were employed to generate plasma at 20.3 kHz. Control experiment of NTP-activated gas phase reaction (*i.e.* empty DBD reactor without a catalyst) was also performed for comparison. According to our previous study [1], the gas phase temperatures in NTP reactor were measured to be at a range of 100–150 °C by using an infrared (IR) thermometer when the applied voltages varied from 6.0 to 7.5 kV.

The outlet gas compositions for both thermal and DBD plasma reactor were measured using a gas chromatograph (GC, PerkinElmer, Clarus® 590) equipped with an Elite-Carbon molecular sieve packed column (N9303926), methaniser, thermal conductivity detector (TCD) and flame ionisation detector (FID). Additionally, a water trap cooled by an ice bath was used to condense any condensable vapours (*e.g.* water) generated by the reaction. A bubble-flow meter was employed to measure the dry gas flow rate of outlet stream in order to determine the CO_2 conversion and selectivity to CH_4 and CO.

For the catalysis under both thermal and NTP conditions, CO_2 (X_{CO2}, %) conversion was calculated using Eq. 1:

$$X_{CO_2} = \frac{F_{CO_2}^{in} - F_{CO_2}^{out}}{F_{CO_2}^{in}} \times 100\% \quad (1)$$

where $F_{CO_2}^{in}$ and $F_{CO_2}^{out}$ are the molar flow rate of CO_2 in the inlet and outlet of the reactor (mol s^{-1}), respectively.

The selectivity to CH_4 (S_{CH_4} , %) and CO (S_{CO}, %) were calculated using Eqs. 2 and 3:

$$S_{CH_4} = \frac{F_{CH_4}^{out}}{F_{CO_2}^{in} - F_{CO_2}^{out}} \times 100\% \quad (2)$$

$$S_{CO} = \frac{F_{CO}^{out}}{F_{CO_2}^{in} - F_{CO_2}^{out}} \times 100\% \quad (3)$$

where $F_{CH_4}^{out}$ and F_{CO}^{out} are the molar flow rate of CH_4 and CO in the outlet of the reactor (mol s^{-1}), respectively.

3. Results and discussion

3.1. Characterisation of catalysts

N_2 adsorption-desorption isotherms of all siliceous zeolite supports (based on silicate-1) are presented in Fig. 1, and the relevant porous properties are summarised in Table 1. All samples show the steep increase in the N_2 uptake at the low relative pressures of $P/P^0 < 0.01$, confirming the presence of micropores in the supports. The physisorption isotherms of S1 and D-S1 resemble the type I isotherm for microporous materials, but with the presence of small hysteresis loops at around $P/P^0 = 0.15$. The existence of the hysteresis loops may be explained by either nitrogen state phase transformation or the fluid-to-crystal-like-phase transition, which has been observed for N_2 adsorption in the micropores of MFI frameworks [24]. Additionally, the isotherm of D-S1 also shows the H4 hysteresis loop that is nearly parallel at $P/P^0 > 0.45$, which is due to the presence of secondary mesopores in D-S1 (introduced by the post-synthesis alkaline treatment of silicalite-1). For the isotherm of the M-S1, it is type IV with a H1 hysteresis loop at relative pressure higher than 0.8, proving the presence of significant mesoporosity. However, due to the templating method used, the mesopores in M-S1 may be non-hierarchical. The M-S1@Shell also shows a type IV isotherm but with a type H2(a) hysteresis loop which closes sharply at $P/P^0 = 0.45$, indicating the presence of inkbottle pores [25, 26]. Such a hysteresis loop is created due to the inkbottle pore structure, where the large pores are accessible *via* the relatively small pores, corresponding to the designed mesopores encapsulated in microporous network structure of the M-S1@Shell.

Table 1. Porous properties of different siliceous zeolite supports by N_2 physisorption analysis.

Zeolite support	S_{BET} [m^2 g^{-1}]	V_{total} [cm^3 g^{-1}]	V_{micro} [cm^3 g^{-1}]
S1	321	0.19	0.13
D-S1	405	0.23	0.11
M-S1	415	0.29	0.11
M-S1@Shell	410	0.27	0.12

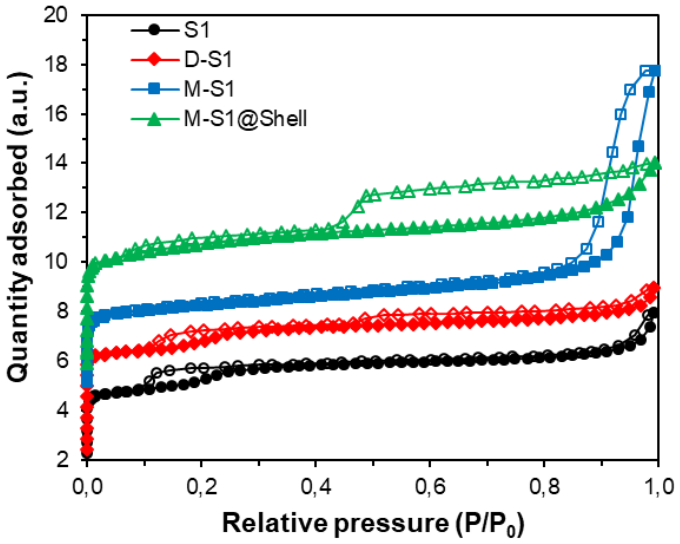

Fig. 1. N_2 adsorption-desorption analysis with offset of 2 mmol g^{-1} between isotherms of silicalite-1 supports with different morphologies.

Fig. 2a shows the powder XRD patterns of the four Ni catalysts supported on different siliceous zeolites prepared in this work, confirming the intactness of the crystalline MFI framework structure after impregnation. In addition to the characteristic peaks of the silicalite-1 supports, as shown in Fig. 2b, XRD patterns of Ni/S1, Ni/M-S1, and Ni/M-S1@Shell catalysts also show the diffraction peaks at *ca.* 2θ = 44.5°, which can be attributed to the Ni species. Conversely, the relevant diffraction peak was not measured by XRD for the Ni/D-S1 catalyst, indicating the possible presence of highly dispersed small Ni nanoparticles on the support, which is likely promoted by the hierarchical mesoporous structure of D-S1 [18]. SEM analysis of the silicalite-1 zeolites are shown in Fig. S1 (Supporting Information, SI), showing that the crystal sizes of the S1 and D-S1 are *ca.* 250 nm, while the M-S1 and M-S1@Shell have the aggregated crystal structures with particle sizes of *ca.* 2 μm.

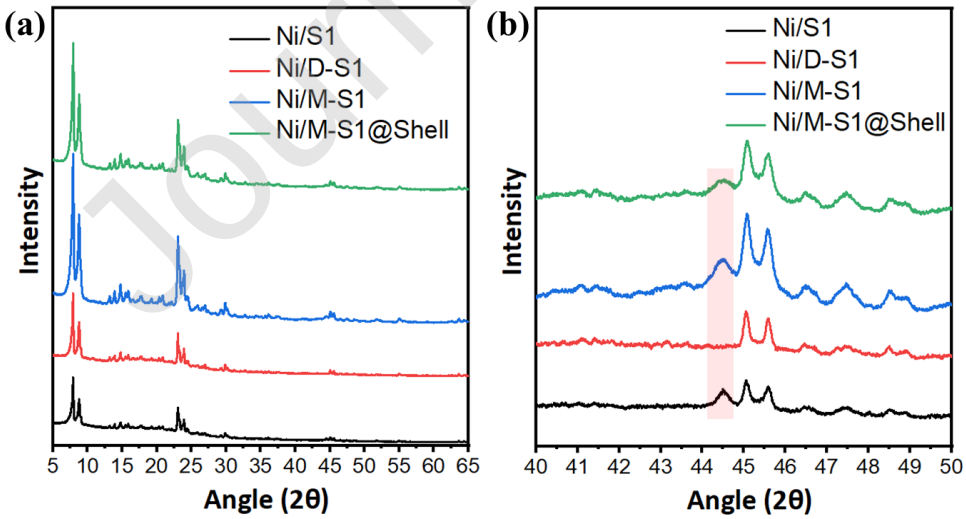

Fig. 2. XRD patterns of the Ni catalysts (5 wt.%) supported on different siliceous zeolites (red rectangle in Fig. 2b corresponds to the Ni species).

TEM analysis of the catalysts was performed to provide the detailed information about the location and dispersion of Ni nanoparticles in the silicalite-1 supports. As shown in Figs. 3a and 3b, for the Ni/S1 catalyst, large and irregularly agglomerated Ni particles are formed mainly on the external surface of microporous silicalite-1 crystals. Such findings regarding the location and morphology of Ni nanoparticles on microporous supports is in line with that of previous studies [18, 27, 28]. For the D-S1 zeolite with the hierarchical meso-micro-porous structure, as shown in Figs. 3d and 3e, it promoted very small Ni nanoparticles with uniform particle sizes primarily inside D-S1 zeolite crystals. Specifically, Fig. 3e shows that Ni nanoparticles are located in the hierarchical network of D-S1 zeolite crystals, suggesting the encapsulated configuration. The mesoporous M-S1 zeolite prepared using the hard-templating method did not promote the Ni metal dispersion very well, resulting in the relatively poorly dispersed and irregularly agglomerated Ni particles in the support (Figs. 3g and 3h). Similarly, as shown in Figs. 3j and 3k, the steam-assisted recrystallised sample of the M-S1@Shell zeolite (*i.e.* the ink bottle pore structure) prompted the irregularly deposition of agglomerated Ni nanoparticles largely situated at the edges of the microporous silicalite-1 layer. Additionally, some Ni nanoparticles can be also observed near the void between M-S1 in the inner layer and microporous silicalite-1 around the zeolite crystals.

Based on the findings of TEM analysis, among all the silicalite-1 supports under study, the hierarchical D-S1 promoted the catalyst (*i.e.* Ni/D-S1) with the relatively small yet well-encapsulated and dispersed Ni nanoparticles inside its framework. Conversely, mainly aggregated Ni particles were formed on other zeolites (*i.e.* S1, M-S1 and M-S1@Shell). The average size of the Ni nanoparticles in Ni/D-S1 is 2.8±0.7 nm (particle size distribution was determined by counting >200 particles, as shown in Fig. 3f), being significantly smaller than that of other catalysts (*i.e.* about 12.9±0.7 nm for Ni/S-1, 26.3±0.7 nm for Ni/M-S1 and 17.8±0.7 nm for Ni/M-S1@Shell, respectively, particle size distribution was determined by counting >100 particles, as shown in Figs 3c, 3i and 3l, respectively).

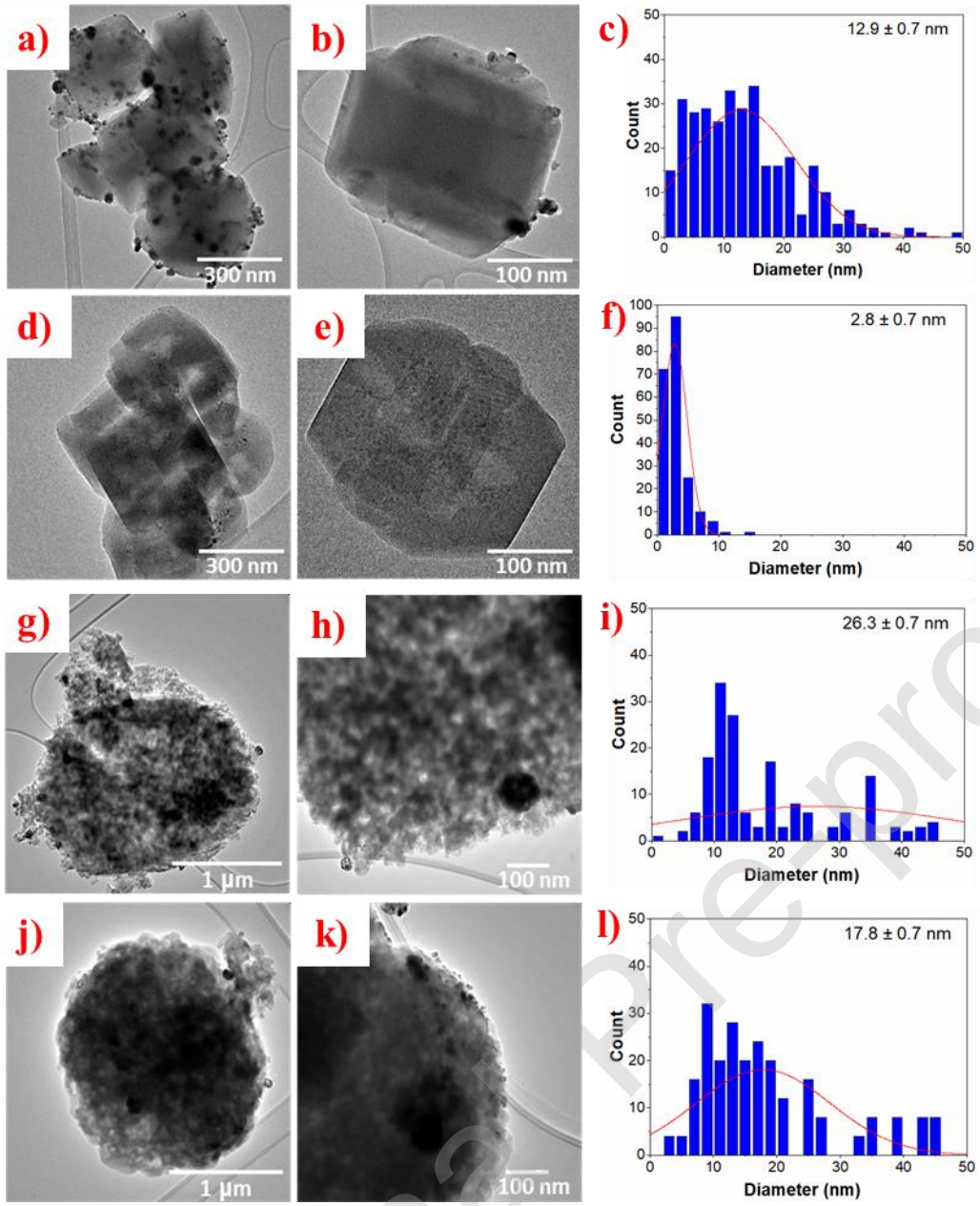

Fig. 3. TEM micrographs of (a-b) Ni/S1, (d-e) Ni/D-S1, (g-h) Ni/M-S1, (j-k) Ni/M-S1@Shell, and (c, f, i, l) corresponding Ni particle size distribution of the catalysts.

3.2. Catalytic CO_2 hydrogenation over the catalysts under thermal and NTP conditions

The catalytic performances of developed catalysts were comparatively assessed using CO_2 hydrogenation (to CH_4) as the model reaction under thermal conditions. Concerning CO_2 conversion and selectivity to CH_4 (as shown in Figs. 4a and 4b), an increase in the system temperature was beneficial to the selective conversion of CO_2 to CH_4 over all the catalysts. The performance of all the systems were rather stable at T ≥450 °C under the conditions used, *i.e.* margins of variation: CO_2 conversion at ± 2% and selectivity to CH_4 at ± 1%. At low temperatures of 250 °C and 300 °C (Fig. 4a), respectively, the Ni/S1 and Ni/M-S1@Shell catalysts presented slightly higher CO_2 conversions than that of the Ni/D-S1 and Ni/M-S1 catalysts, indicated that the

reactants (*i.e.* CO_2 and H_2) might only interact with Ni species sitting on the external surface of zeolite crystals. Conversely, at high temperatures from 350 °C to 500 °C, the Ni/D-S1 catalyst outperformed other three catalysts. This can be explained by (*i*) the improved diffusivity of gaseous reactants (into the pores of zeolite supports to interact with Ni species located inside zeolite crystals) at elevated temperatures (for example, the diffusivity (D_{eff}) of CO_2 in 5A zeolite is doubled by raising the temperature from 261 °C to 325 °C, *i.e.* from 0.74×10^2 cm^{-2} s to 1.40×10^2 cm^{-2} s) [29], (*ii*) the high dispersion of small Ni nanoparticles in the Ni/D-S1 catalyst (Figs. 3d, 3e and 5a), and (*iii*) the hierarchical porous network of D-S1. Additionally, in Fig. 4a, the measured CO_2 conversions of the Ni/D-S1 catalyst at 450 and 500 °C were slightly higher than the corresponding equilibrium conversions. This could be mainly attributed to the measurement errors incurred by GC analysis and measurement of gas flow rate (*via* a bubble flow meter).

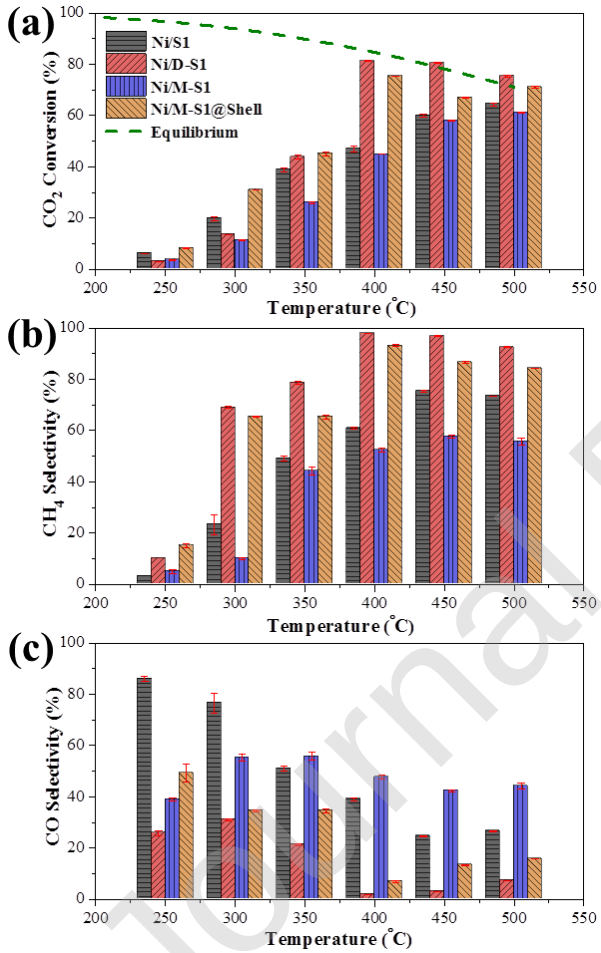

Fig. 4. Catalytic CO_2 hydrogenation performance over the Ni/S1, Ni/D-S1, Ni/M-S1 and Ni/M-S1@Shell catalysts under thermal conditions: (a) CO_2 conversion, (b) CH_4 selectivity, and (c) CO selectivity (experimental conditions: feed gas composition of $H_2/CO_2 = 4$, GHSV of 30,000 mL (STP) g_{cat}^{-1} h^{-1}, temperature of 250–500 °C). Equilibrium conversions of the reaction in Figs. 4a are calculated using Aspen Plus 8.0.

Regarding the selectivity to CH_4, as shown in Fig. 4b, the Ni/D-S1 and Ni/M-S1@Shell catalysts outperformed the Ni/S1 and Ni/M-S1 catalysts over the studied range of temperatures. The Ni/M-S1 catalyst showed relatively the high selectivity to CO at 40–58% (*i.e.* 47.4±6.9%, Fig. 4c),

suggesting that the accessibility of the encapsulated Ni catalyst was significantly impeded due to the enclosed mesopores structure of the M-S1 support. For the Ni/S1, Ni/D-S1 and Ni/M-S1@Shell catalysts, the elevated temperatures (*i.e.* ≥400 °C) was beneficial to suppress the unwanted CO production, as shown in Figs. 4b and 4c. The Ni/D-S1 catalyst presented the highest CO_2 conversion of *ca.* 80% at 450 °C, being comparable to the corresponding equilibrium conversion. The Ni dispersion and metallic surface area of different catalysts were measured by H_2 pulse chemisorption, and the results are presented in Fig. 5a. The Ni/D-S1 catalyst demonstrated comparatively the highest Ni dispersion and metallic surface area (*ca.* 2.5% and 17 m^2 g_{Ni}^{-1}), being significantly higher than that of other catalysts under investigation, *e.g.*, 0.5% and 3 m^2 g_{Ni}^{-1} for Ni/M-S1. These results are in line with results regarding Ni particle size distribution by TEM (Fig. 3). In general, the catalytic performance of the catalysts in CO_2 hydrogenation under thermal conditionals correlates well with the Ni dispersion results at high temperatures of ≥450 °C (Fig. 5b).

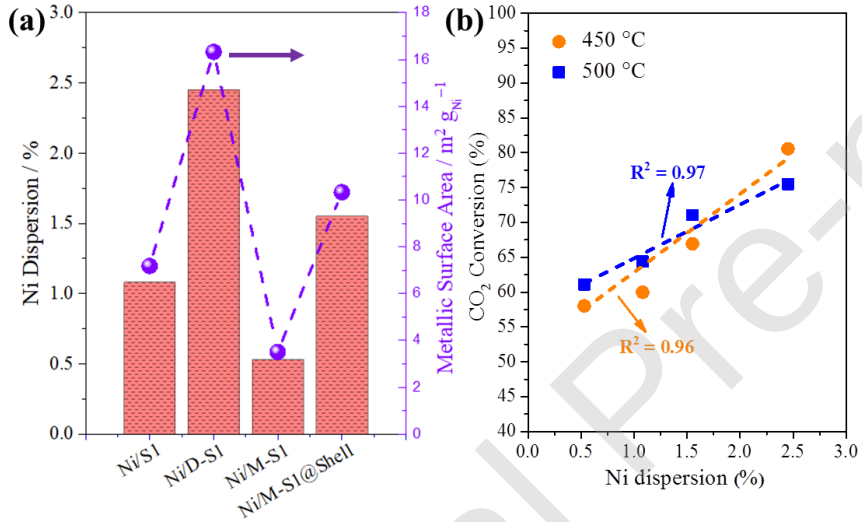

Fig. 5. (a) Ni dispersion and metallic surface area of the catalysts under study, (b) linear fittings of CO_2 conversion *vs.* Ni dispersion.

In situ diffuse reflectance infrared Fourier-transform spectroscopy-mass spectrometry (DRIFTS-MS) was performed to probe the possible reaction mechanism of the thermal catalytic systems under study. As shown in Figs. 6a–6d, by increasing the temperature from 40 to 400 °C continuously, similar system dynamics were recorded for all catalysts, *i.e.* (*i*) the intensity of the IR band at *ca.* 2,349 cm^{-1} (the gas phase CO_2, shaded by the red rectangle) diminished gradually; (*ii*) the adsorbed surface carbonyl (characterised by the IR band at *ca.* 2,019 and 1,850 cm^{-1}) on Ni^0 sites and carbonate species (characterised by the IR bands at *ca.* 1,537 and 1,360 cm^{-1}) on Ni^{2+} from the remaining NiO appeared progressively [30, 31]. The findings by *in situ* DRIFTS suggest that CO_2 was mainly converted into CO on the Ni surface at low temperatures of <300 °C, explaining the high selectivity to CO (Fig. 4c) [32]. However, due to the dissociation of hydrogen at high temperature, surface formyl (HCO*) was formed on the surface of all the catalysts (*ca.* 1,760 cm^{-1},

shaded by the blue rectangle). With an increase of the temperature, the C-O band cleavage might occur on the Ni/D-S1 and Ni/M-S1@Shell catalysts at temperatures >300 °C, leading to the formation of surface CH_x species, which is evidenced by the appearance of the IR band at ~3,000 cm^{-1} on their surfaces (Figs. 6b and 6d). Comparatively, the IR band related to CH_x species on the Ni/S1 and Ni/M-S1 catalysts are rather weak, especially the Ni/M-S1 (Fig. 6c), on which it can hardly be observed under conditions used. In this case, surface CO* species was more likely to act as a key intermediate for the co-production of CO and CH_4, wherein the reaction towards CH_4 may proceed *via*: CO* → HCO* → CH_x without C–O bond scission reaction.

The corresponding MS profiles (Fig. 7) of the *in situ* DRIFTS catalysis confirmed that CH_4 was the main product in the catalytic thermal system using the Ni/D-S1 (Fig. 7b) and Ni/M-S1@Shell (Fig. 7d) catalysts compared to other two catalysts. Specifically, the Ni/D-S1 catalyst showed the shortest emerging time (*ca.* 35 min) of the line at m/z = 16 (corresponding to methane), compared to that of the Ni/S1 (*ca.* 45 min) and Ni/M-S1@Shell (*ca.* 40 min) catalysts. It should be noted that only a small amount of methane was detected in the catalytic system using the Ni/M-S1 catalyst (Fig. 7c), whereas CO (m/z = 28) was observed as the main product. The results from the *in situ* DRIFTS-MS characterisation are in line with the catalytic performances discussed above, confirming the comparatively good performance of Ni/D-S1 and Ni/M-S1@Shell in the thermally activated CO_2 hydrogenation than Ni/S1 and Ni/M-S1. It was found that, at low reaction temperatures (*e.g.* 250 °C, as show in Fig. 4), the total selectivity to CO and CH_4 did not reach 100%. The coupled DRIFTS-MS analysis showed the production of other side products from the system (*i.e.* CO_2 hydrogenation over Ni/DS-1 at 250 °C), *i.e.* the MS signals at m/z = 29 and 31, suggesting the production of methanol and formic acid during the catalysis. Since the work cofuses the conversion of CO_2 into CH_4, the detailed analysis of the selectivity and yield of the liquid products were not performed. Exemplified by Ni/DS-1, the carbon balances of the catalytic systems at ≥300 °C are 96 ± 1% (Fig. S4a).

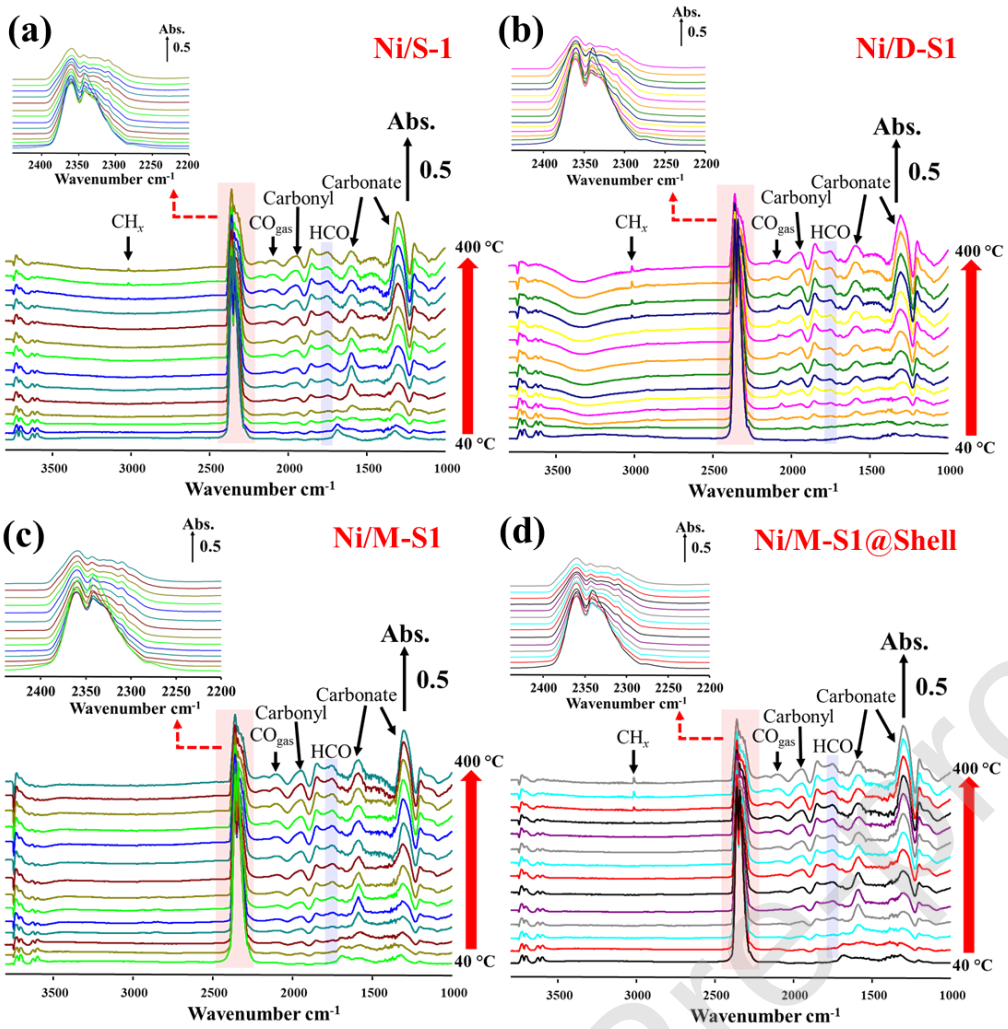

Fig. 6. In-situ DRIFTS spectra of CO_2 methanation over the (a) Ni/S-1, (b) Ni/D-S1, (c) Ni/M-S1, and (d) Ni/M-S1@Shell catalysts under thermal conditions (feed gas mixture = 10 vol.% CO_2/40 vol.% H_2 in Ar balance, total flow rate = 50 mL min^{-1}).

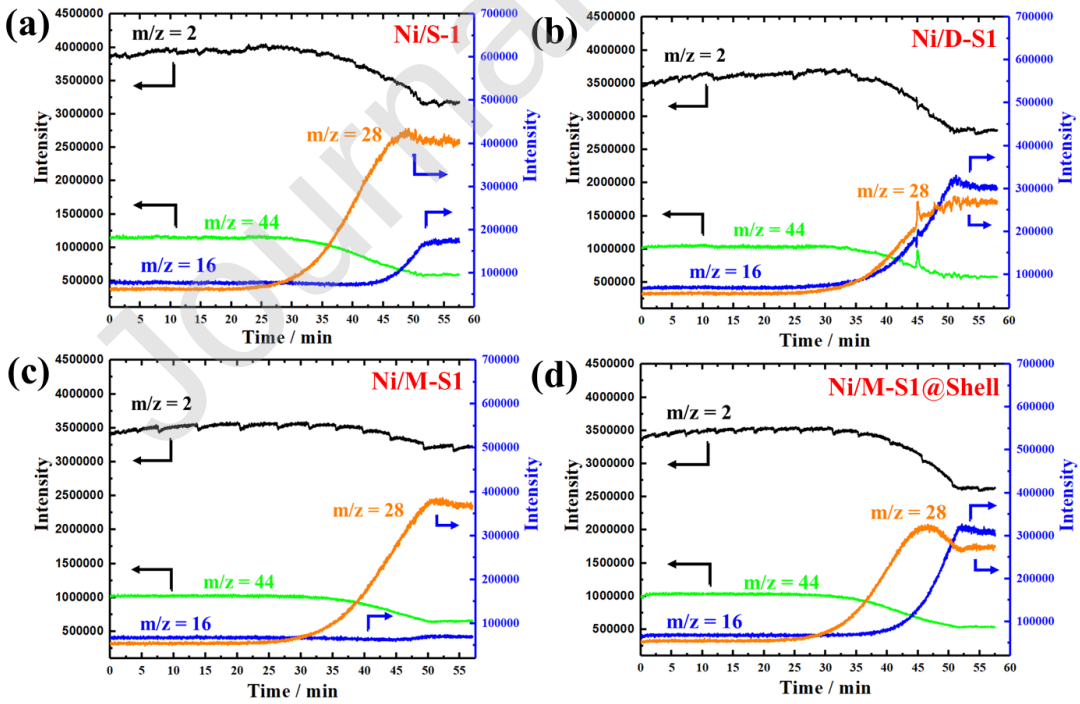

Fig. 7. MS signals of the in situ DRIFTS system as a function of time-on-stream during the thermally activated catalytic CO_2 hydrogenation over the (a) Ni/S-1, (b) Ni/D-S1, (c) Ni/M-S1, and (d) Ni/M-S1@Shell catalysts (feed gas mixture = 10 vol.% CO_2/40 vol.% H_2 in Ar balance, total flow rate = 50 mL min^{-1}).

To understand the effect of metal dispersion and support structure of Ni supported on silicalite-1 catalysts on the catalysis under NTP conditions, the comparative investigation of NTP activated catalytic CO_2 hydrogenation was performed. Under the NTP conditions in absence of a catalyst (the control experiment, as shown in Fig. S2), the CO_2 conversion (*ca.* 5–10 %) and selectivity to CH_4 (about zero) were insignificant with CO as main product (due to the NTP-induced CO_2 dissociation in the gas phase [1, 33]).

Fig. 8a shows the comparison of the absolute CO_2 conversion of the reaction over the catalysts activated by NTP. Both CO_2 conversion and selectivity to CH_4 were improved with an increase in the input energy, *i.e.* the applied voltage, especially over Ni/D-S1 catalyst. This can be explained by the increased density of reactive species in the discharge space (*i.e.* availability) due to the strengthened input energy. Previous study has shown that the existence of abundant reactive species in the NTP-catalysis system could significantly promote the reactions [34]. Under NTP conditions, collisions between high temperature electrons and reactant molecules, leading to their dissociation, and hence the formation of reactive species in the gas phase, which can participate in the surface reactions over the catalyst. The lifetime of electronically-excited species in NTP systems are normally short, depending on the specific input energy. In general, under atmospheric pressure condition, the mean free path and time interval between collisions is *ca.* 100 nm and *ca.* 1 ns, respectively [16]. Accordingly, the plasma-induced reactive species may lose their energy due to collisional quenching, especially at a low applied voltage. Therefore, the availability and accessibility of such reactive species to the catalyst surface are crucial to the surface reactions under the plasma conditions.

By analysing CO_2 conversions in detail, the effect of the pore structure of the supports and the characteristics of Ni particles on the zeolite supports can be found. At applied voltages of 6.0, 6.5, and 7.0 kV, the Ni/D-S1 and Ni/M-S1 catalysts with encapsulated Ni species were less active than the Ni/S1 and Ni/M-S1@Shell catalysts (in which the Ni species sit primarily on the outer surface of the supports). It indicates that, with a limited availability of NTP induced short-lived species in the gas phase, they might primarily interact with the exposed catalyst surface with less diffusion resistance (compared to the encapsulated catalysts). Conversely, at a high applied voltage of 7.5 kV, the abundant presence of the reactive species in the system facilitated their diffusion to the encapsulated catalyst surface. Accordingly, the Ni/D-S1 catalyst demonstrated the highest activity with a CO_2 conversion of *ca.* 75%, while the other catalysts showed the comparable results (*i.e.* CO_2 conversions at ~50%).

Based on the measured selectivity to CH_4, the CH_4 selective pathway of the catalysis was enabled at ≥6.5 kV under plasma conditions. However, the improvement in CH_4 selectivity of the Ni/M-S1 catalyst was insignificant, only by 5%, whereas by 50% for the Ni/D-S1 catalysts. Under the NTP conditions, Ni/M-S1 was not selective to CH_4, suggesting that the pore structure of M-S1 support, *i.e.* enclosed mesopores, reduced the accessibility of the encapsulated Ni catalyst significantly. Consequently, the reactions might mainly be in the gas phase, and hence being not selective to CH_4. Conversely, the D-S1, which possesses the hierarchical pore structure, with the well dispersed Ni particles in its network, promoted the diffusion of reactive species into the network, as well as the interaction with the active Ni species. As shown in Fig. 8b, at a low applied voltage of 6.0 kV, all catalysts present low CH_4 selectivity (*i.e.* <10%), while CO as main product was detected with relatively high selectivity at *ca.* 38–50%. Again, carbon balances of gaseous products from the systems at 6.0 kV are poor due to methanol and formic acid formation (Fig. S3b), and at applied voltage of ≥6.5 kV), the carbon balance is 95.7 ± 1.5% (as shown in Fig. S4b).

Regarding the order of activity of the catalysts under study, *i.e.* CO_2 conversion, the ranking of the catalysts under both thermal and NTP conditions are rather similar, *i.e.* Ni/D-S1 was the most active catalyst, outperforming Ni/S1, Ni/M-S1 and Ni/M-S1@Shell, which showed comparable performances. Regarding the selectivity to CH_4 (Fig. 8b), Ni/D-S1 also showed the high performance of ~98% at an applied voltage of 7.5 kV under the plasma condition, being comparable to that under thermal conditions (*i.e.* ~96% at T ≥ 450 °C, Fig. 4b). Under both conditions, Ni/M-S1 catalyst presented the comparably worst CH_4 selectivity. Overall, the experimental findings of this work revealed that both the intrinsic nature of the metal catalyst (*i.e.* dispersion) and the porous structurer of the support are critical factors for the catalysis under the NTP conditions, exemplified by the model system of catalytic CO_2 hydrogenation to CH_4. Findings of the present show that the catalyst with the relatively high Ni dispersion can be highly beneficial to the catalysis under both thermal and NTP conditions. Therefore, the development of relevant catalysts with highly dispersed metal active sites (*e.g.* sub-nanosized clusters, even single-atoms/sites, not limited to Ni), and study of their performance in catalysis, especially in the integrated NTP-catalyst, deserve further investigation.

Additionally, the use of porous Ni/D-S1 catalyst in the discharge zone improved the intensity of current pulses (red line in Fig. S5), indicating the improved discharge and plasma generation, being similar to the phenomena observed in the integrated NTP-catalysis system using the catalysts based on MOFs [14]. Regarding the energy efficiency of the NTP-catalysis system (EE, defined by Eq. S2), the Ni/D-S1 catalyst showed the highest EE value of ~4.4 mmol kJ^{-1} at an applied voltage of 7.5 kV under the plasma condition (as shown in Fig. S6), being significantly higher than other catalysts under the NTP conditions (e.g., ~0.5 mmol kJ^{-1} for Ni/M-S1).

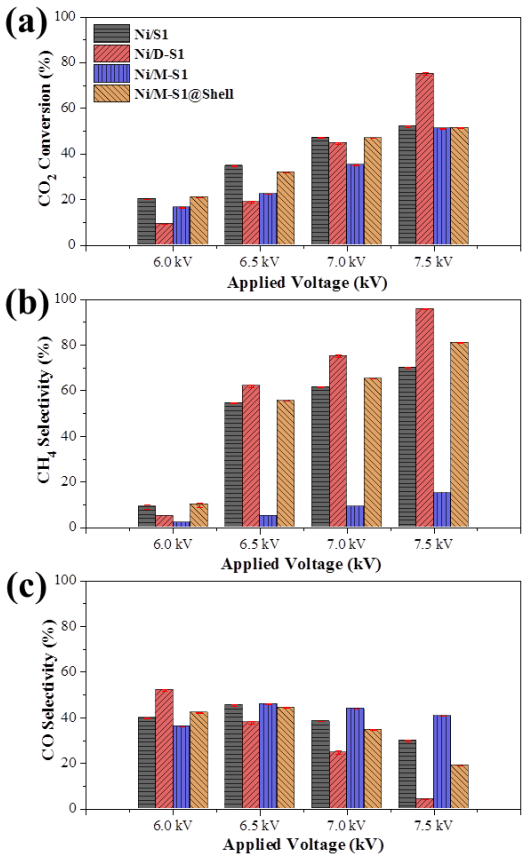

Fig. 8. Catalytic CO_2 hydrogenation performances over the Ni/S1, Ni/D-S1, Ni/M-S1 and Ni/M-S1@Shell catalysts under NTP conditions: (a) CO_2 conversion, (b) CH_4 selectivity, and (c) CO selectivity (experimental conditions: feed gas composition of $H_2/CO_2 = 4$, GHSV of 30,000 mL (STP) g_{cat}^{-1} h^{-1}, applied peak voltage of 6.0–7.5 kV, frequency of 20.3 kHz).

A comprehensive understanding of the role of a catalyst in the integrated NTP-catalysis system is challenging due to its complex nature. Based on the findings presented above from both characterisation and comparative catalytic assessments (under the thermal and NTP conditions), one can reveal it to some extent. Heterogeneous catalysis under thermal conditions is well explained which undergoes the diffusion of reactants, adsorption of reactants on the surface of catalysts, surface reactions and desorption of formed products. Accordingly, the developed catalysts showed the corresponding performance in CO_2 hydrogenation under the thermal conditions, *i.e.* an increase in the reaction temperature resulted in the improved molecular diffusion and the accelerated surface reactions. Since the reactions have to occur on the surface of Ni catalysts, at elevated temperatures (T ≥450 °C) under steady state, the structure of the porous support, as well as the associated diffusion tortuosity, are less effective on the conversion of CO_2 (Fig. 4a). The resulting differences in the selectivity (Figs. 4b and 4c) can be attributed to the characteristics of the supported Ni catalysts, *i.e.* the metal dispersion and particle size [35].

Conversely, under the NTP conditions, at the high input energy (the existence of abundant short-lived reactive species is common), the dissociation of reactants may mostly occur in the gas phase

(by the collision of high energy electrons to give the reactive species) instead of on the surface of the catalyst. Previous studies showed that (*i*) the plasma generation is only possible in pores with the diameter greater than the Debye radius (typically >3 μm, depending on the discharge gas) [36] and (*ii*) the electrical discharge cannot penetrate the micropores of <0.8 μm to generate microdischarges [16, 37]. Hence, the plasma-induced reactive species cannot be formed inside the micropores of silicalite-1 (~0.5 nm). Consequently, the diffusion of the short-lived reactive species in the porous support is relatively important, *i.e.* they may be quenched before reaching the surface of catalysts. For the catalysts under study, Ni/D-S1 possesses the hierarchical pore network, benefiting the accessibility of the Ni catalyst to the short-lived species (as indicted by Fig. 9b). Ni species supported on S1 and M-S1@Shell are mainly on the external surface of the supports, being readily accessible (as indicted by Figs. 9a and 9d). Conversely, for M-S1, its hierarchical enclosed pores hinder the diffusion of reactive species to the surface of the enclosed Ni particles, leading to the comparatively low CO_2 conversion (in comparison with that of Ni/M-S1 catalysed CO_2 hydrogenation under the thermal conditions). More importantly, the significantly low selectivity to CH_4 of Ni/M-S1 under the NTP conditions suggests the possible non-selective gas-phase reactions (Fig. 9c). Under the NTP conditions where the accessibility of Ni catalyst is not an issue, the nature of the supported catalysts micro-meso-porous materials is again the dominating factor, determining the performance of the catalysis. It is also worth mentioning that, in addition to the aspects regarding the catalyst design discussed above, the investigation to study the relevant discharge characteristics of plasma after the integration with the catalyst (*e.g.* by analysing Lissajous figures [38]) is necessary as well, which can be highly beneficial to gain insights into the NTP-catalyst interaction and develop the integrated NTP-catalyst system toward practical application. Also, the energy consumption aspect of the NTP-catalysis system deserves further optimisation. For example, preliminary energy consumption analysis of the NTP-catalysis and conventional thermal catalysis system was performed with Ni/D-S1. As shown in Fig. S7, the NTP-catalysis system showed a higher electric energy consumption (EC, defined by Eq. S3) at ~6.5×10^5 kJ mol^{-1} at 6.0 kV (Fig. S7b) than that of the thermal catalysis at ~1.5×10^5 kJ mol^{-1} (at 300 °C), which could be attributed to the low CH_4 selectivity of NTP-catalysis system at a relatively low voltage of 6.0 kV (*i.e.* <10%, Fig. 8). However, at high applied voltages of ≥6.5 kV, EC values of the NTP-catalysis system are comparable to that of the thermal catalysis system, *i.e.* <1.5×10^5 kJ mol^{-1}. Therefore, considering the energy efficiency of NTP-catalysis, the design of bespoke catalysts for NTP-catalysis with high CH_4 selectivity and yield, especially at low applied voltages, is needed. Importantly, the explicit technical and economic analysis (TEA) of the developed NTP-catalysis system (especially the energy consumption in comparison with the conventional thermal counterpart) is also necessary to assess the potential of NTP-catalysis towards practical applications.

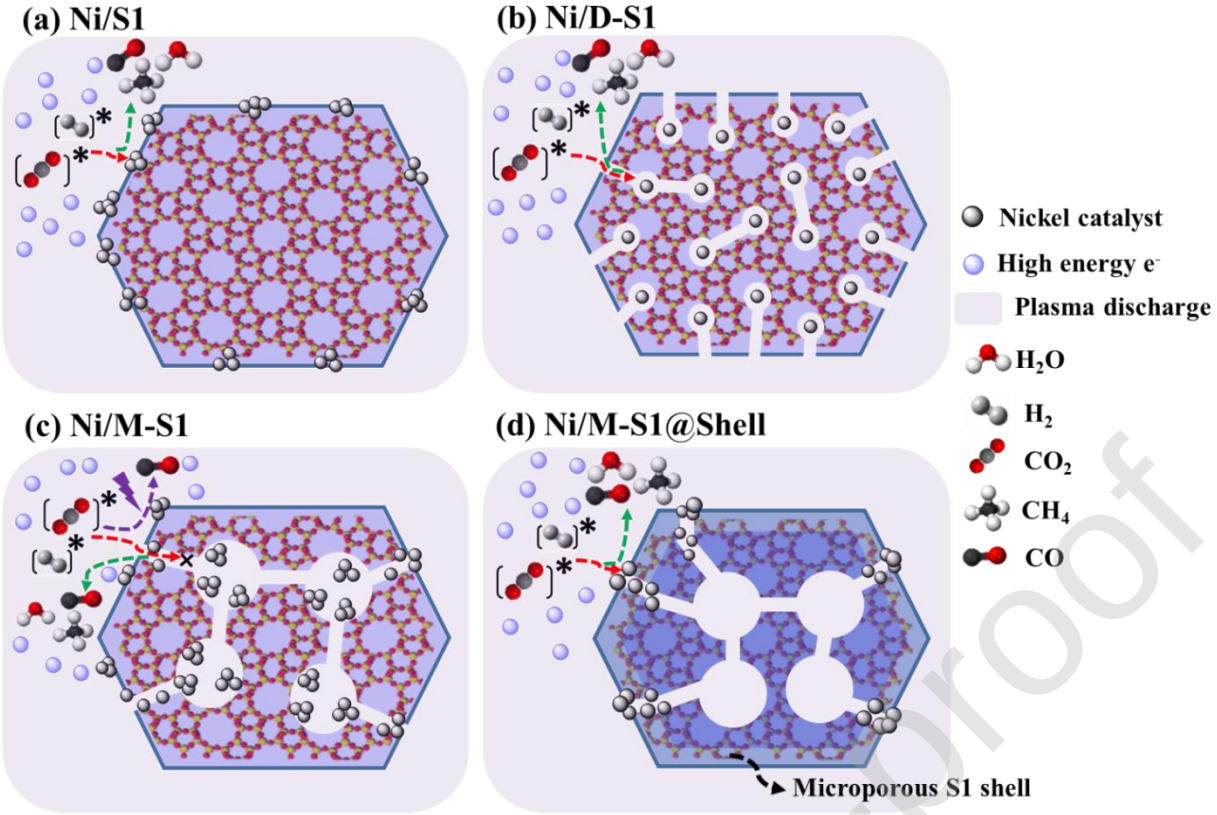

Fig. 9. Mechanistic scheme of catalytic CO_2 hydrogenation over different catalysts under NTP conditions: (a) Ni/S1, (b) Ni/D-S1, (c) Ni/M-S1, and (d) Ni/M-S1@Shell.

4. Conclusions

However, the mechanism of the integrated NTP-catalysis system is complex which requires significant effort of research to elucidate. One of the specific parameters of the system is the lifetime of the reactive gaseous species which plays an important role in the efficiency of the plasma-catalyst system regarding the conversion and selectivity. In this work, siliceous silicalite-1 zeolites were synthesised with different porous properties, which were then used to support Ni catalyst with different features regarding the location, size and dispersion Ni species in the supports. The catalysts were then employed to study the effect the intrinsic nature of the catalysts, accessibility of the active sites and the porous structures on the performance of CO_2 hydrogenation under both thermal and plasma conditions. The comparative investigation showed that the hierarchical meso-micro-porous structures and the associated well-dispersion Ni species were highly beneficial to the catalysis under the NTP conditions, especially at relatively high voltages. The findings of the work suggest that (*i*) the porous structure of the catalyst support and the location of catalytic active sites in the porous support determines the accessibility of the metal sites to the plasma-generated reactive gaseous species, affecting the performance of the NTP-catalyst system significantly and (*ii*) the intrinsic property of the metal catalysts such as particle sizes and

dispersion is crucial under both thermal and NTP conditions. This work demonstrates the effect of catalyst design on the NTP activated catalysis, exemplified by catalytic CO_2 hydrogenation over supported Ni catalysts, paves the way to the further development of bespoke porous materials supported metal catalysts for NTP-catalyst system.

Credit Author Statement

The contribution of authors are:

XF and SK conceptualised the research and provioded resoruces for the work.

HC, FG and YM performed the experiemntal work under the supervision of CH, SK amd XF.

HC, YM and SC contributed to in situ DRIFTS-MS characterisaion of the catalysis under the supervision of XF and CH.

FJ and JJM contributed to the catalyst design and relevant characerisation under the supervision of SK.

HC drafted the initial manuscript.

TS and BM helped the discussion.

SK, CH and XF revised the manuscript.

Declaration of Interest Statement

On behalf of all authors, I confirm here that the authors contribuetd to this work have no conflict of interest.

Acknowledgements

This project has received funding from European Union's Horizon 2020 research and innovation programme under grant agreement No. 872102. HC thanks the financial support from the European Commission Marie Skłodowska-Curie Individual Fellowship (grant agreement No. 748196). SK,

FG and JM thanks Independent Research Fund Denmark (Grant Nos. 5054-00119 and 6111-00237), Villum fonden (Grant No. 13158), and Haldor Topsøe A/S for financial support.

References:

[1] H. Chen, Y. Mu, Y. Shao, S. Chansai, S. Xu, C.E. Stere, H. Xiang, R. Zhang, Y. Jiao, C. Hardacre, X. Fan, Coupling non-thermal plasma with Ni catalysts supported on BETA zeolite for catalytic CO2 methanation, Catalysis Science & Technology, 9 (2019) 4135-4145.
[2] H. Chen, Y. Mu, Y. Shao, S. Chansai, H. Xiang, Y. Jiao, C. Hardacre, X. Fan, Nonthermal plasma (NTP) activated metal–organic frameworks (MOFs) catalyst for catalytic CO2 hydrogenation, AIChE Journal, 66 (2020) e16853.
[3] S. Xu, S. Chansai, Y. Shao, S. Xu, Y.-c. Wang, S. Haigh, Y. Mu, Y. Jiao, C.E. Stere, H. Chen, X. Fan, C. Hardacre, Mechanistic study of non-thermal plasma assisted CO2 hydrogenation over Ru supported on MgAl layered double hydroxide, Applied Catalysis B: Environmental, 268 (2020) 118752.
[4] A. Parastaev, W.F.L.M. Hoeben, B.E.J.M. van Heesch, N. Kosinov, E.J.M. Hensen, Temperature-programmed plasma surface reaction: An approach to determine plasma-catalytic performance, Applied Catalysis B: Environmental, 239 (2018) 168-177.
[5] X. Tu, J.C. Whitehead, Plasma-catalytic dry reforming of methane in an atmospheric dielectric barrier discharge: Understanding the synergistic effect at low temperature, Applied Catalysis B: Environmental, 125 (2012) 439-448.
[6] C.E. Stere, J.A. Anderson, S. Chansai, J.J. Delgado, A. Goguet, W.G. Graham, C. Hardacre, S.F.R. Taylor, X. Tu, Z. Wang, H. Yang, Non-Thermal Plasma Activation of Gold-Based Catalysts for Low-Temperature Water–Gas Shift Catalysis, Angewandte Chemie International Edition, 56 (2017) 5579-5583.
[7] R. Vakili, R. Gholami, C.E. Stere, S. Chansai, H. Chen, S.M. Holmes, Y. Jiao, C. Hardacre, X. Fan, Plasma-assisted catalytic dry reforming of methane (DRM) over metal-organic frameworks (MOFs)-based catalysts, Applied Catalysis B: Environmental, (2019) 118195.
[8] L. Wang, Y. Yi, H. Guo, X. Tu, Atmospheric Pressure and Room Temperature Synthesis of Methanol through Plasma-Catalytic Hydrogenation of CO2, ACS Catalysis, 8 (2018) 90-100.
[9] H.-H. Kim, A. Ogata, M. Schiorlin, E. Marotta, C. Paradisi, Oxygen Isotope (18O2) Evidence on the Role of Oxygen in the Plasma-Driven Catalysis of VOC Oxidation, Catalysis Letters, 141 (2011) 277-282.
[10] U. Roland, F. Holzer, A. Pöppl, F.D. Kopinke, Combination of non-thermal plasma and heterogeneous catalysis for oxidation of volatile organic compounds: Part 3. Electron paramagnetic resonance (EPR) studies of plasma-treated porous alumina, Applied Catalysis B: Environmental, 58 (2005) 227-234.
[11] E.K. Gibson, C.E. Stere, B. Curran-McAteer, W. Jones, G. Cibin, D. Gianolio, A. Goguet, P.P. Wells, C.R.A. Catlow, P. Collier, P. Hinde, C. Hardacre, Probing the Role of a Non-Thermal Plasma (NTP) in the Hybrid NTP Catalytic Oxidation of Methane, Angewandte Chemie, 129 (2017) 9479-9483.
[12] C.E. Stere, W. Adress, R. Burch, S. Chansai, A. Goguet, W.G. Graham, C. Hardacre, Probing a Non-Thermal Plasma Activated Heterogeneously Catalyzed Reaction Using in Situ DRIFTS-MS, ACS Catalysis, 5 (2015) 956-964.
[13] S. Xu, S. Chansai, C. Stere, B. Inceesungvorn, A. Goguet, K. Wangkawong, S.F.R. Taylor, N. Al-Janabi, C. Hardacre, P.A. Martin, X. Fan, Sustaining metal–organic frameworks for water–gas shift catalysis by non-thermal plasma, Nature Catalysis, 2 (2019) 142-148.
[14] R. Vakili, R. Gholami, C.E. Stere, S. Chansai, H. Chen, S.M. Holmes, Y. Jiao, C. Hardacre, X. Fan, Plasma-assisted catalytic dry reforming of methane (DRM) over metal-organic frameworks (MOFs)-based catalysts, Applied Catalysis B: Environmental, 260 (2020) 118195.
[15] J. Kim, D.B. Go, J.C. Hicks, Synergistic effects of plasma–catalyst interactions for CH4 activation, Physical Chemistry Chemical Physics, 19 (2017) 13010-13021.
[16] J.C. Whitehead, Plasma-catalysis: Is it just a question of scale?, Frontiers of Chemical Science and Engineering, 13 (2019) 264-273.
[17] P.A. Christensen, A.H.B.M. Ali, Z.T.A.W. Mashhadani, M.A. Carroll, P.A. Martin, The Production of Ketene and C5O2 from CO2, N2 and CH4 in a Non-thermal Plasma Catalysed by Earth-Abundant Elements: An In-Situ FTIR Study, Plasma Chemistry and Plasma Processing, 38 (2018) 461-484.
[18] F. Goodarzi, L. Kang, F.R. Wang, F. Joensen, S. Kegnæs, J. Mielby, Methanation of Carbon Dioxide over Zeolite-Encapsulated Nickel Nanoparticles, ChemCatChem, 10 (2018) 1566-1570.
[19] F. Goodarzi, R.P. Thumbayil, K. Enemark-Rasmussen, J. Mielby, T.T.M. Nguyen, P. Beato, F. Joensen, S. Kegnæs, Enhanced Catalytic Performance of Zn-containing HZSM-5 upon Selective Desilication in Ethane Dehydroaromatization Process, ChemCatChem, 12 (2020) 1519-1526.
[20] C.J.H. Jacobsen, C. Madsen, J. Houzvicka, I. Schmidt, A. Carlsson, Mesoporous Zeolite Single Crystals, Journal of the American Chemical Society, 122 (2000) 7116-7117.
[21] J. Mielby, J.O. Abildstrøm, S. Perez-Ferreras, S.B. Rasmussen, S. Kegnæs, Formation of pyridine N-oxides using mesoporous titanium silicalite-1, Journal of Porous Materials, 21 (2014) 531-537.

[22] K.H. Rasmussen, F. Goodarzi, D.B. Christensen, J. Mielby, S. Kegnæs, Stabilization of Metal Nanoparticle Catalysts via Encapsulation in Mesoporous Zeolites by Steam-Assisted Recrystallization, ACS Applied Nano Materials, 2 (2019) 8083-8091.
[23] S. Chansai, R. Burch, C. Hardacre, H. Oh, W.S. Epling, An investigation of the role of surface nitrate species in the oxidation of propene on a Pt-based diesel oxidation catalyst, Catalysis Science & Technology, 3 (2013) 2349-2356.
[24] P.L. Llewellyn, J.P. Coulomb, Y. Grillet, J. Patarin, H. Lauter, H. Reichert, J. Rouquerol, Adsorption by MFI-type zeolites examined by isothermal microcalorimetry and neutron diffraction. 1. Argon, krypton, and methane, Langmuir, 9 (1993) 1846-1851.
[25] M. Thommes, Physical Adsorption Characterization of Nanoporous Materials, Chemie Ingenieur Technik, 82 (2010) 1059-1073.
[26] J.C. Groen, J. Pérez-Ramírez, Critical appraisal of mesopore characterization by adsorption analysis, Applied Catalysis A: General, 268 (2004) 121-125.
[27] D. Laprune, A. Tuel, D. Farrusseng, F. Meunier, Selective removal of external Ni nanoparticles on Ni@ silicalite-1 single crystal nanoboxes: Application to size-selective arene hydrogenation, Applied Catalysis A: General, 535 (2017) 69-76.
[28] J.O. Abildstrøm, M. Kegnæs, G. Hytoft, J. Mielby, S. Kegnæs, Synthesis of mesoporous zeolite catalysts by in situ formation of carbon template over nickel nanoparticles, Microporous and Mesoporous Materials, 225 (2016) 232-237.
[29] Y.H. Ma, C. Mancel, Diffusion studies of CO2, NO, NO2, and SO2 on molecular sieve zeolites by gas chromatography, AIChE Journal, 18 (1972) 1148-1153.
[30] A. Westermann, B. Azambre, M.C. Bacariza, I. Graça, M.F. Ribeiro, J.M. Lopes, C. Henriques, Insight into CO2 methanation mechanism over NiUSY zeolites: An operando IR study, Applied Catalysis B: Environmental, 174-175 (2015) 120-125.
[31] E. Gallei, G. Stumpf, Infrared spectroscopic studies of the adsorption of carbon dioxide and the coadsorption of carbon dioxide and water on CaY- and NiY-zeolites, Journal of Colloid and Interface Science, 55 (1976) 415-420.
[32] M. Agnelli, H.M. Swaan, C. Marquez-Alvarez, G.A. Martin, C. Mirodatos, CO Hydrogenation on a Nickel Catalyst: II. A Mechanistic Study by Transient Kinetics and Infrared Spectroscopy, Journal of Catalysis, 175 (1998) 117-128.
[33] S. Xu, J.C. Whitehead, P.A. Martin, CO2 conversion in a non-thermal, barium titanate packed bed plasma reactor: The effect of dilution by Ar and N2, Chemical Engineering Journal, 327 (2017) 764-773.
[34] Y.-R. Zhang, K. Van Laer, E.C. Neyts, A. Bogaerts, Can plasma be formed in catalyst pores? A modeling investigation, Applied Catalysis B: Environmental, 185 (2016) 56-67.
[35] F. Goodarzi, D.B. Christensen, F. Joensen, S. Kegnæs, J. Mielby, The effect of active site distribution in bi-functional Pt-zeolite catalysts for ethane dehydroaromatization, Applied Catalysis A: General, (2020) 117383.
[36] A. Fridman, Plasma chemistry, Cambridge university press2008.
[37] H.-H. Kim, Y. Teramoto, N. Negishi, A. Ogata, A multidisciplinary approach to understand the interactions of nonthermal plasma and catalyst: A review, Catalysis Today, 256 (2015) 13-22.
[38] I. Biganzoli, R. Barni, A. Gurioli, R. Pertile, C. Riccardi, Experimental investigation of Lissajous figure shapes in planar and surface dielectric barrier discharges, Journal of Physics: Conference Series, 550 (2014) 012039.